



VORTEX STRUCTURE INVESTIGATION BY LDV
FOR TWO ROTOR BLADE TIPS IN FORWARD FLIGHT

BY

B.M.J. BEESTEN

DEPARTMENT OF AEROSPACE ENGINEERING
RWTH AACHEN, UNIVERSITY OF TECHNOLOGY
AACHEN, GERMANY

AND

U. SEELHORST

INSTITUTE FOR FLUID MECHANICS
GERMAN AEROSPACE RESEARCH ESTABLISHMENT DLR
GÖTTINGEN, GERMANY

TWENTIETH EUROPEAN ROTORCRAFT FORUM
OCTOBER 4 - 7, 1994 AMSTERDAM

VORTEX STRUCTURE INVESTIGATION BY LDV FOR TWO ROTOR BLADE TIPS IN FORWARD FLIGHT

B.M.J. Beesten¹, U. Seelhorst²

¹ Department of Aerospace Engineering
RWTH Aachen, University of Technology
D-52056 Aachen, Germany

² Institute for Fluid Dynamics
DLR
D-37073 Göttingen, Germany

Abstract

The measurement of local flow vectors at positions near the helicopter rotor were performed with a three component Laser-Doppler-Velocimeter (3D LDV). The new conception of 3D-LDV brought good progress concerning sensitivity, data rate and third component resolution. A 'position monitoring system' gave access to blade motion parameters (lead-lag motion, pitching and angle of incidence) at any chosen radial position of the blade, where LDV measurements were performed. The measurements gave principle results concerning the structure of a blade tip vortex in forward flight condition. For example the vortex core radius has been obtained as well as the speed of vortex roll up. Since the tests were run with two different blade tips, a regular square tip for reference and a non-planar tip called winglet, the influence of these winglets on vortex structure and BVI behaviour was investigated. In addition to the vortex parameter like location of the vortex relative to the rotor plane, vortex core size, axial velocity, vortex strength and vorticity the 3D-LDV measurements yield results concerning the orientation of the vortex axis in space, 3D-vorticity and the temporal roll up of the different blade tip vortices.

Nomenclature

BVI	blade-vortex interaction	x, y, z	co-ordinates
DLR	German Research Establishment	u, v, w	velocity components
FFT	Fast Fourier Transformation	z	axial position
ILR	Aachen department of aerospace eng.	$z_{1,2}$	blade vortex miss distance
LDV	laser doppler velocimeter	Γ	circulation
RWTH	Aachen University of Technology	Ω	rotor frequency
R	rotor radius	β	rotor tilt angle
U_0	wind tunnel velocity	ϑ_{coll}	collective pitch
$V_{convect}$	vonvection velocity	ϑ_{cycl}	cyclic pitch
c	chord	μ	advance ratio
c_T	rotor thrust coefficient	ρ	air density
l	convected distance	σ	rotor solidity
n	rotor rotational speed	ψ	azimuth
r	radial position	ψ_0	trigger azimuth
r_c	vortex core radius	ω	vorticity
t	time	$\omega_x, \omega_y, \omega_z$	vorticity components

1. Introduction

The investigation of the noise emission of helicopters became more and more important within the last decade. Therefore helicopter noise has been subject of many research projects [1]. Blade-Vortex-Interactions (BVI) are known as a major source of impulsive noise (Fig.1). Under approach and landing flight conditions when BVI-noise occurs near the ground, its reduction is of special interest.

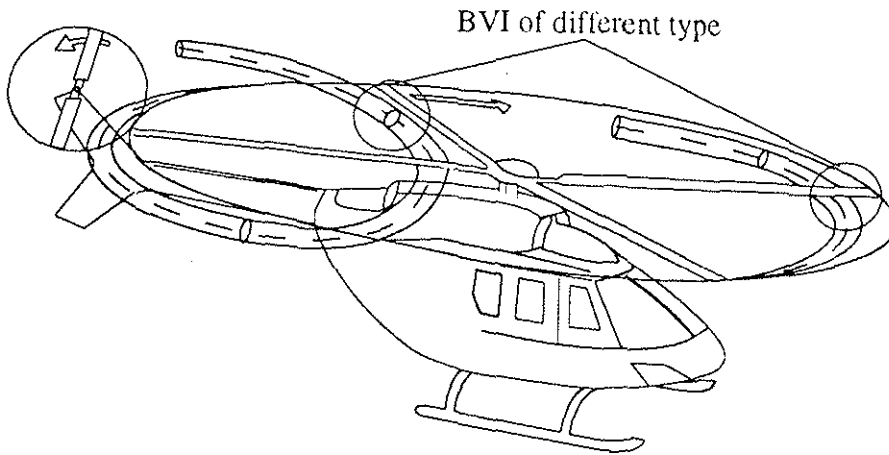


Fig.1 Blade-vortex-interactions

As BVI-noise is governed by the induced velocities of tip vortices, it depends on blade-vortex miss distance, vortex strength and vortex structure. A reduction of noise levels requires a decrease in velocities induced on the rotor. Possible approaches are to reduce the vortex strength, to modify the vortex structure (e.g. by increasing the vortex core size) or to enlarge the blade-vortex miss distance. The increase of blade-vortex miss distance was found to be the most efficient approach to reduce BVI-noise [2]. A way to increase the miss distance is the use of non-planar blade tips. Different shapes of non-planar blades have been developed since the early eighties in France [3] and Germany [4]. In Aachen the influence of downward pointing blade tips has been investigated in detail. The so called winglets use two mechanisms to reduce BVI-intensity. Like Fig. 2 illustrates the tip vortex rolls up some distance underneath the rotor plane. This results in a significantly enlarged miss distance. Furtheron winglets effect on the vortex structure. This results in lower induced velocities due to a less concentrated vortex.

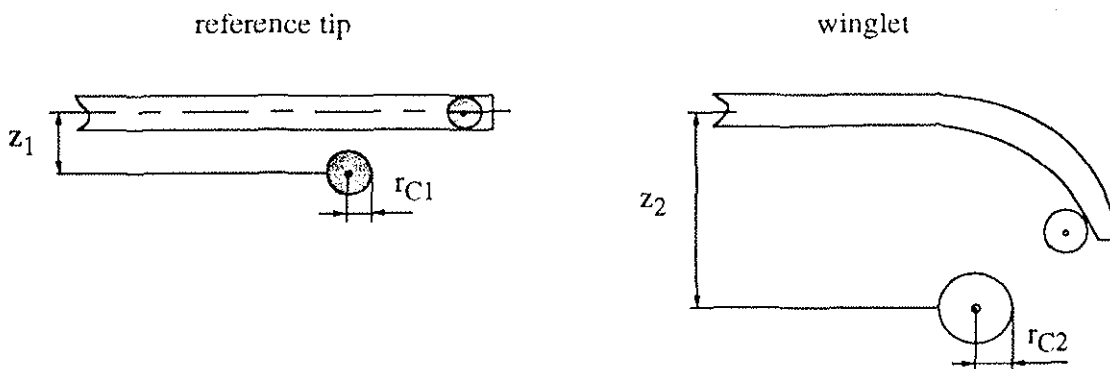


Fig. 2 Mechanisms of BVI reduction

The measurement of vortex structures behind rotor blades has been of high interest for many years. This interest even increased with the attempts to modify the vortex structure. When a new three component Laser-Doppler-Velocimeter was developed by the Institute for Fluid Dynamics of the DLR, a co-operative programme between RWTH and DLR was set up to measure vortex structures behind two blade tips in forward flight condition. These tests using the mobile LDV of DLR were run in the ILR Aachen low speed wind tunnel during summer 1993. LDV is a very useful tool to investigate the flow field in a rotating helicopter rotor, because it is a non intrusive measurement technique, which is able to take measurements within the rotor plane. It should be pointed out that the flow field of a helicopter in forward flight is highly unsteady. But due to the periodicity of the flow field it is possible to sample data over several rotor revolutions if the measurements are triggered accurately.

2. Experimental set up

2.1 Blade geometries

Fig.3 presents the blade tips tested in the co-operative programme. As a reference configuration Blade No.1 was used. It has a planar rectangular shape and uses an untwisted NACA 0015 airfoil. The second blade tested was Aachen's blade No.3, the twisted winglet. It has a swept-back tip for better high speed characteristics. The nose is extended in forward direction to improve lift characteristics at the retreating blade and to avoid additional pitching moments caused by the sweep. The non-planarity, defined as the distance between the blade tip and the rotor plane, has a value of about 0.65 chord lengths. Twisting starts at a radius of 91% and reaches 7° at the tip. This gives extra bound circulation at the tip region and pushes the vortex further downward.

Both blades are made of carbon/glass-fibre-composites and have NACA 0015 airfoil sections of 0.054 m main chord length. This gives the four-bladed rotor a solidity of about 0.105.

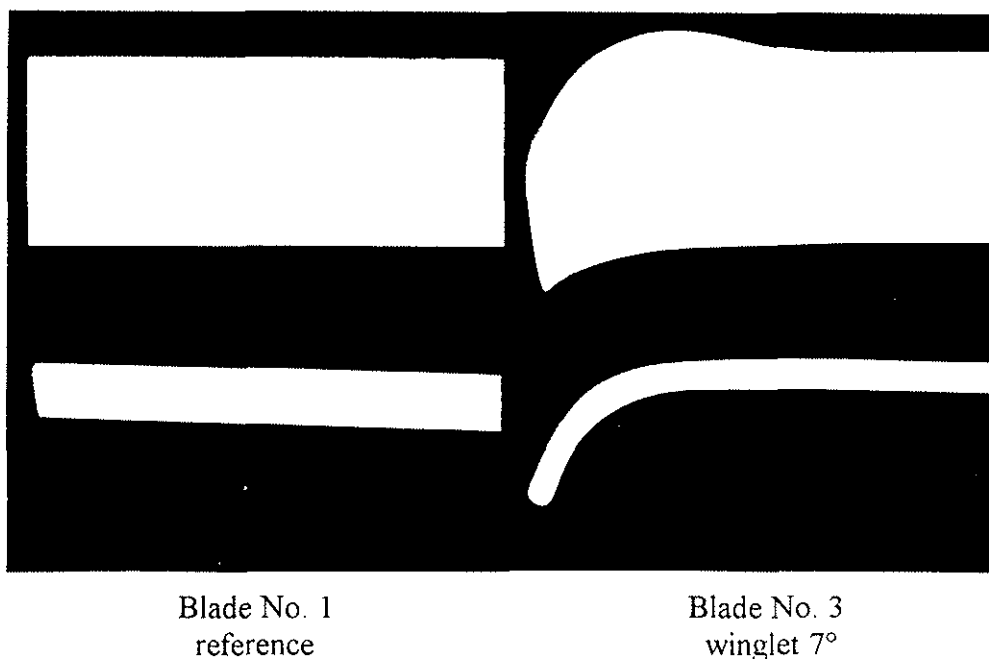


Fig. 3 Blade tip shapes

2.2 Test facility

These tests were performed in the open test section of the ILR Aachen low-speed wind tunnel. Fig.4 shows the test set-up including the LDV system. A four-bladed model rotor with a diameter of 1.02 m was driven by a 65 KW engine. The rotor was fully articulated and had flapping hinges.

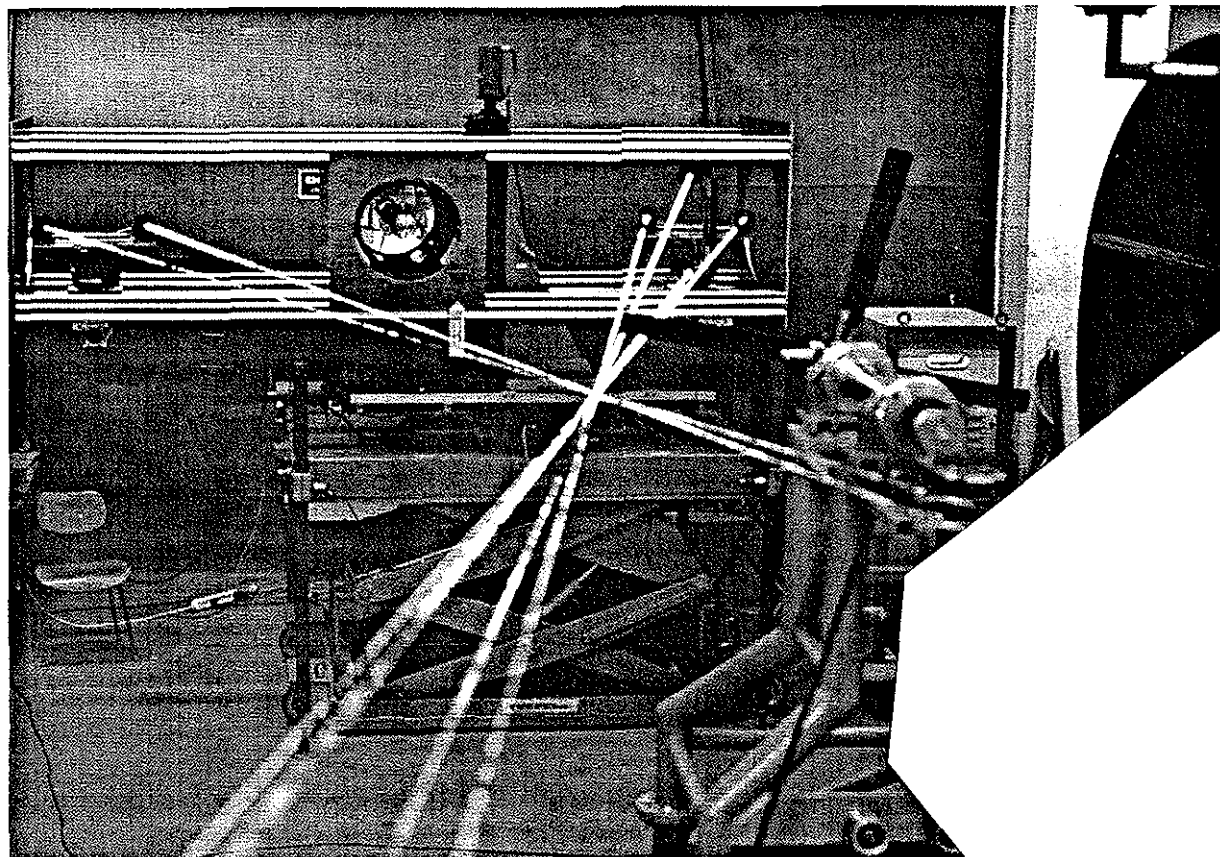


Fig. 4 Test set up

2.3. LDV system

To investigate the flow field within the plane of a rotating helicopter model rotor, a nonintrusive measuring technique has to be used. In addition, to examine the exact structure of the flow field including a blade tip vortex 3-dimensional measurements are necessary. The three component laser-Doppler-velocimeter used for the investigation of the blade tip vortex flow field has been developed at the Institute for Fluid Mechanics of the DLR [5]. Fig. 5 shows the schematic set-up of the 3D LDV.

The 3D LDV system operates in back scatter, off-axis mode. A 6 Watt Argon-Ion Laser is used as light source. The three most intensive laser lines (476.5 nm, 488 nm and 514.5 nm) are utilised to distinguish the different velocity components in the LDV velocity system. Each of the laser beams is divided into two individual beams with similar intensity, one superimposed with a Bragg shift of 40 MHz, to determine also the direction of the flow vector for this component. The laser beams are coupled into single mode glass fibres and with individual transmitting optics they are launched into the probe volume. This is done by a Dantec

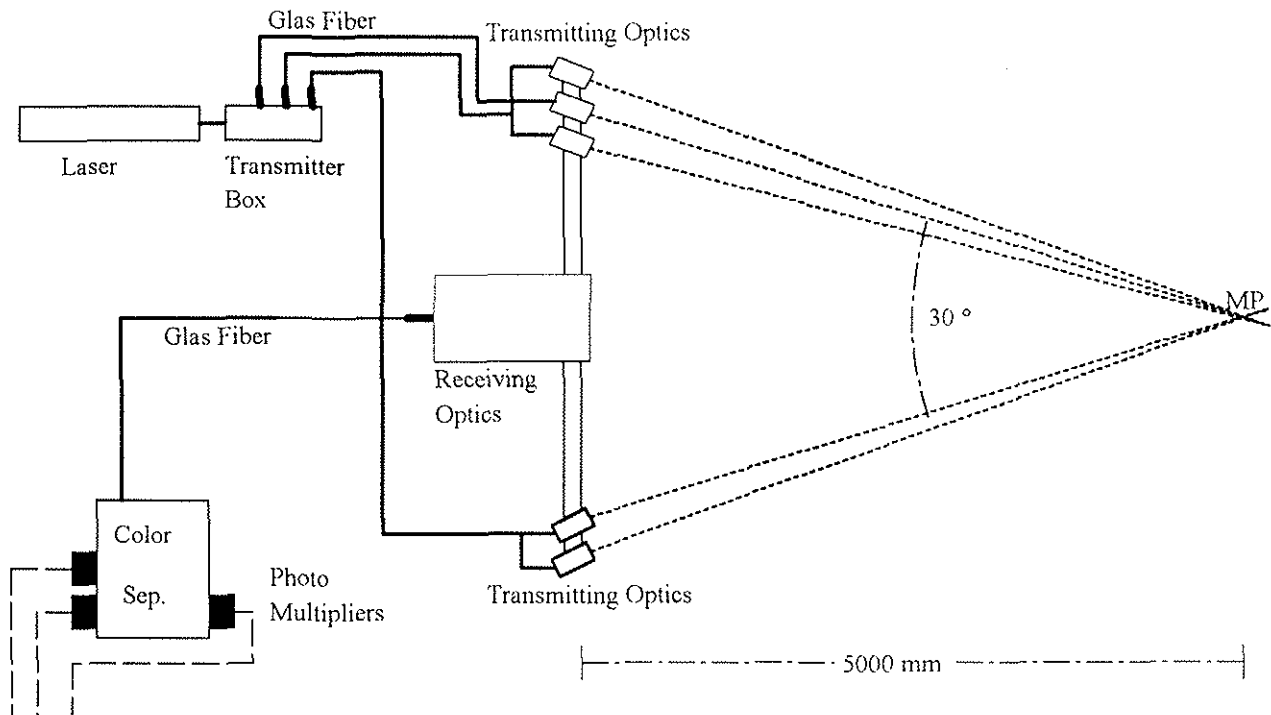


Fig. 5 LDV system

transmitter box, type 60X41 and Dantec transmitting optics, type 41X171. For good resolution of the third velocity component the angle between the optical axis is about 30° . The effective size of the probe volume is about 0.25 mm in diameter and 1mm in length. Particles, necessarily induced into the flow, consist of dispersed oil, having a maximum size lower than $1 \mu\text{m}$. These particles are small enough to follow the flow in the correct manner [6].

Because of the difference in the efficiency of light scattering between forward and backward Mie-scattering in the range of 10^3 , the receiving optics of the LDV system, operating in backward scatter mode, require a large aperture to gather an adequate portion of scattered light to realize a sufficient high data rate. As the working distance of the LDV is flexible, two different receiving optics can be integrated into the system. One with an aperture of 350 mm and a working distance from 3 m to 5 m, the other one with an aperture of 500 mm and a fixed working distance of 5m. The gathered scattered light, containing the information of all the three individual velocity components is coupled into a multi mode glass fibre, which leads the light to a prism system, where it is divided into the single wavelength and then converted into an electrical signal by a PM tube.

Data acquisition

The obtained Doppler bursts are filtered and digitised. A Fast Fourier Analysis (FFT) of the Doppler burst leads to the frequency, which is directly proportional to the velocity of the particle, from which the scattered light occurs. This is done for each channel by a DSA 3220 from Aerometrics. If the signals on each of the three components coincide, the obtained velocities are stored together with the time information and afterwards converted from the non orthogonal LDV velocity system into the orthogonal wind tunnel velocity system.

Data evaluation

Proceeding on the assumption of a periodic flow field with respect to the rotor revolution, conditional sampling is used to get time depending information of the flow field. A trigger signal from the rotor axis can be shifted with a time delay to any chosen azimuth position of

the rotor blade with an accuracy of 0.3%. At this position the clock of the data acquisition system is set to zero. Data acquisition is started now for a time window, corresponding to a preselected azimuth window or a time needed for the flow structure to pass through the probe volume. Usually data are acquired just within a small azimuthal window of the whole rotor revolution. Converting time information into spatial information can be done in two different ways. The transformation of the time information to an azimuth angle is done with the simple equation:

$$(1) \quad \Psi = \Psi_0 + (360 \cdot n \cdot t)$$

The transformation of the time information into a spatial information of the flow structure is done by the convection velocity of the structure:

$$(2) \quad l = V_{\text{convect}} \cdot t$$

Using the conditional sampling mode to acquire time depending velocity data, which is afterwards converted into spatial velocity data, leads to an unaccuracy in this spatial information. This is due to the fact, that the flow structures changes during the measuring time. This unaccuracy is acceptable, because the data acquisition in conditional sampling mode reduces the total measurement time. This factor consist of the number of space fixed LDV measurement co-ordinates, multiplied by the number of intervals, in which the time information is divided.

Position monitoring

Simultaneous to the velocity data acquisition the position of the rotor blade has to be acquired. This is done for each revolution at the azimuth angle Ψ_0 , where the trigger from the rotor axis starts the LDV measurements. The position monitoring system, developed at the Institute for Fluid Mechanics of the DLR [7], is used for this purpose. With this system it is possible to evaluate the pitching and the lead lag motion with an accuracy of 0.1mm, as well as the angle of attack of the blade at one azimuth position.

3. Test parameter

Before discussing the locations of the measurements the co-ordinate systems used shall be introduced. Like Fig. 6 shows x points in wind tunnel direction (against flight direction) and y in down wash direction. The orientation of the vorticity components can be seen as well.

Since wind tunnel time was rather limited just one flight condition could be investigated. So the advance ratio was selected to $\mu = 0.2$ as a medium speed flight where BVI occur. To get strong tip vortices the collective was set to $\vartheta_{\text{coll}} = 10.0^\circ$ which gives a highly loaded rotor with an approximate $c_T = 0.008$. Cyclic was set to $\vartheta_{\text{cycl}} = 3.5^\circ$ to trim the rotor. The shaft angle has been $\beta = -3.0^\circ$. Rotor speed was selected to $n = 1500$ rpm.

Measurements were performed in two planes perpendicular to the rotor plane. Fig. 7 gives their locations. Plane I was selected to measure the undisturbed vortex structure of the tip vortices of both blades. It is located at 0° of azimuth and the wind tunnel velocity moves the vortex away from the rotor. A second reason led to this location. The probe volume was traversed just in y-direction while x-variation resulted from time dependent measurements and

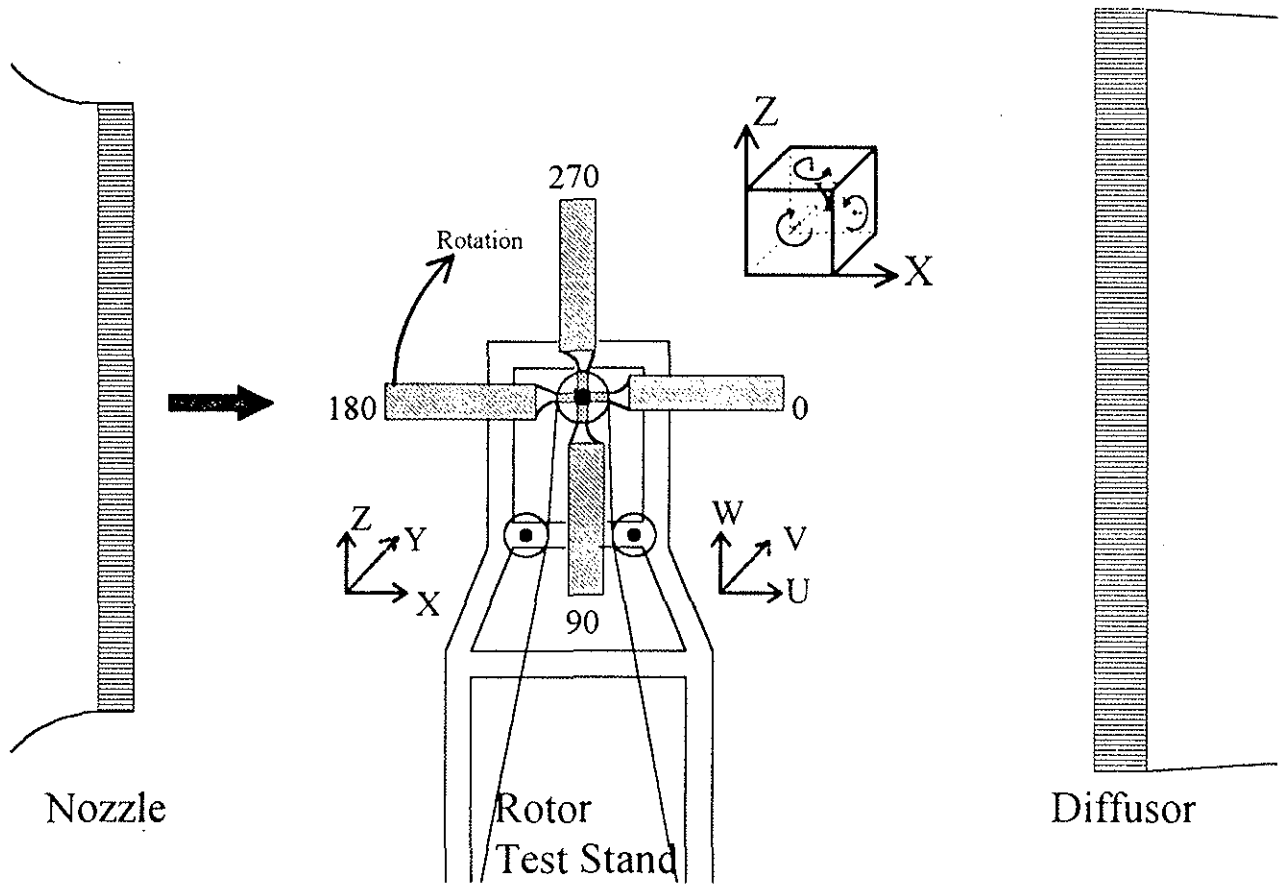


Fig. 6 Co-ordinate systems

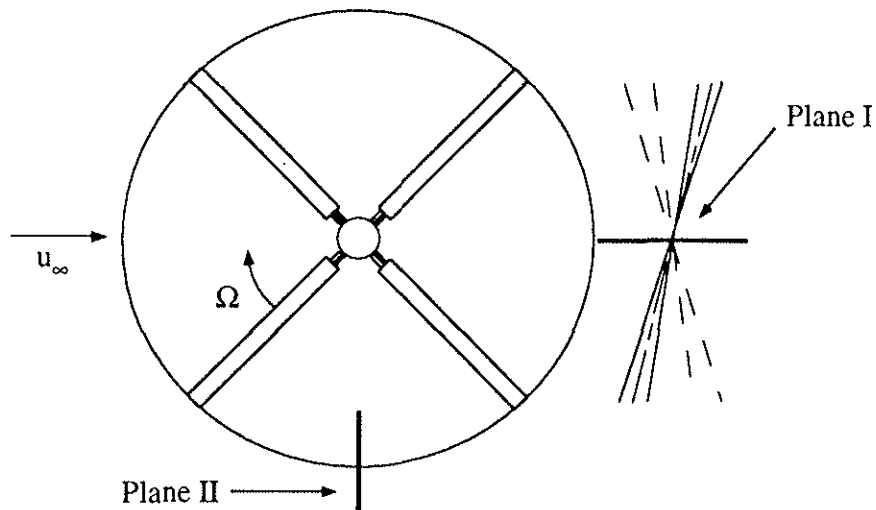


Fig. 7 Measurement location

the wind tunnel convection. By this method the age of the vortex differs a bit with x-position but ensuring the vortex has rolled up completely the accuracy is sufficient. The advantage of the method can be seen in the fact that the measuring time is reduced by 95%. The exact location of the LDV probe volume for the measurements of the undisturbed vortex at 0° azimuth the probe volume was 50 mm in x-direction outboard the rotor plane. From this point, at different positions in y-direction 3D-LDV measurements were performed in an azimuth

window of 60°, corresponding to a time of 6.6 ms. During this time the tip vortex generated at 0° passes through the probe volume driven by the wind tunnel and downwash convection velocity. Time depending velocity data at measuring location I (0° azimuth) are converted into a spatial fixed co-ordinate system by equation (2).

Measurement in plane II were performed to investigate the vortex roll up and the BVI characteristics of the different blades. Here just a coarse grid of 6 x 11 points could be measured with about 50 time (azimuth) steps. It has to be noted that the coarse grid reduces the accuracy of the results. Zero location of the co-ordinate system in y and z direction is at the blade tip, with the blade at 90° azimuth angle. Data acquisition starts, when the blade is located at an azimuth angle of 85° and stops at a blade azimuth position of 108°. This corresponds with a distance of one chord in front and two chords behind the blade. This azimuth window is divided into 50 single intervals, which lead to a resolution in azimuth of better than 0.5°. The total measuring grid around the blade exists of a cube of 50 by 11 by 6 points. The data acquisition in conditional sampling mode reduces the total measuring time by 98% for the grid. For measuring location II (90° azimuth) the transformation of time depending data in co-ordinate fixed data was realized using equation (1).

Vorticity calculation

The evaluation of the single components of the vorticity (ω_x , ω_y , ω_z) is performed by calculating:

$$(3) \quad \omega_i = \frac{1}{2} \text{rot}(\bar{u}_i)$$

for the center of a rectangle with data points on each corner. The definition of the orientation of the single components of the vorticity is illustrated in Fig. 6.

4. Results

4.1 vortex structure

The exact positions of the vortex structure measurements are pointed out in Fig. 8. A first coarse grid of 20 mm spacing has been refined in the region of the estimated vortex location. A minimum spacing of 2.5 mm in the center of the grid has been realized with 14 y-positions in total.

Vector plots were first obtained from the measurements to give an impression of the flow field and to check the measurements. The vector plots in Fig. 9 give the vortex location and its extent.

Further on it can be seen from Fig. 9 that the grid refinement did not catch the vortex core exactly. Specially the center of the reference tip vortex has been missed by the finer grid. Unfortunately no data in the real center of the vortices are available to measure the exact vortex parameter like core radius or maximum tangential velocities for example. In Fig. 10 those measurements of the tangential velocities are presented that come closest to the vortex center.

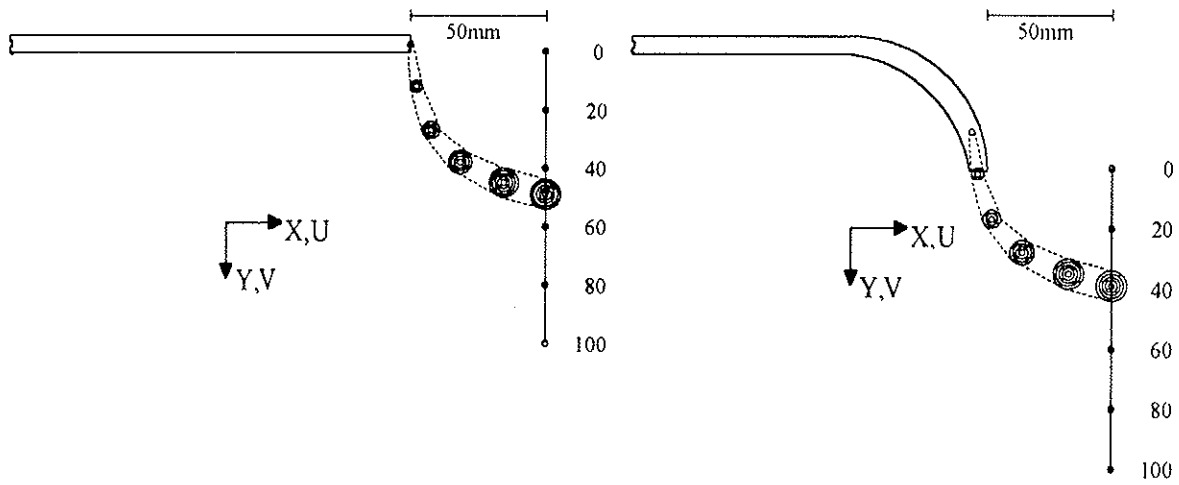


Fig. 8 Grid at 0°

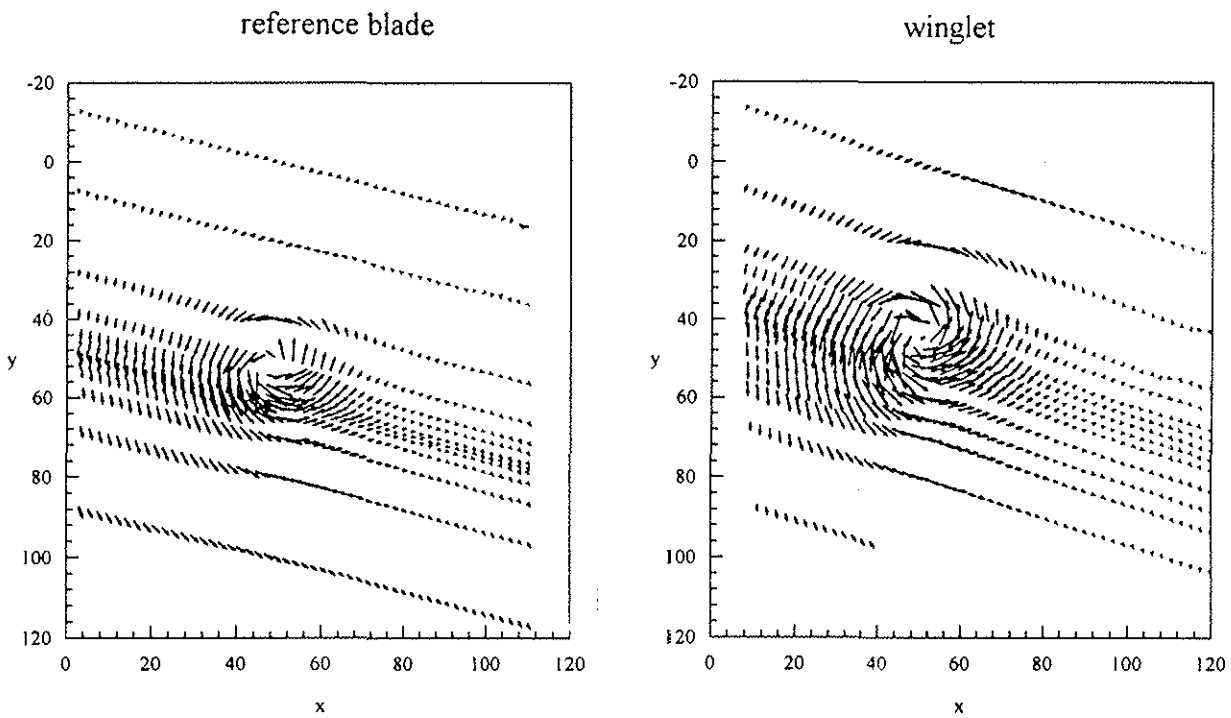


Fig. 9 Vector plots

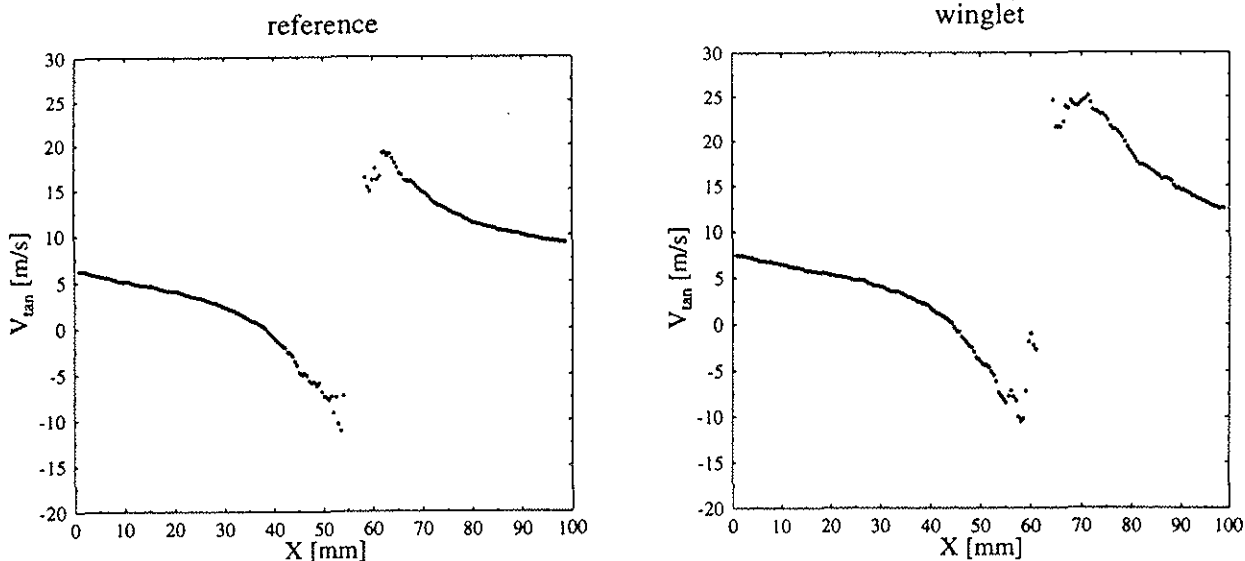


Fig. 10 Tangential velocities

From these data the vortex core radius of the reference tip vortex has been estimated to 8.9% of the blade chord or 0.94% of the rotor radius. The result for the winglet vortex is 7.8% chord. The unexact measurement location underestimates the core radius of the reference tip. To explain the difference between both blades a more precise look at the vortex structure is required. Neither the vector plots nor the velocity profiles allow detailed statements about the vortex structure. More information can be obtained from vorticity plots.

Fig. 11 shows that the reference blade vortex is significantly more concentrated than the winglet one. So the maximum vorticities are found to be 5190 s^{-1} for the reference blade and 4180 s^{-1} for the winglet. The difference is expected to be even larger in most flight conditions, because during these tests the collective was held constant for both blade types although winglets are known to produce more lift per collective pitch [8]. Consistently the circulation of the reference vortex was found to be lower ($0.786 \text{ m}^2/\text{s}$) than that of the winglet ($0.846 \text{ m}^2/\text{s}$). Comparing both vorticity contours it should be recognized that the winglet vortex shows two centers of vorticity and is far away from being rotary symmetric. This explains the unexpected lower core radius with the winglet. The two centers are explained by a double vortex that occurs with downward pointing winglets [9].

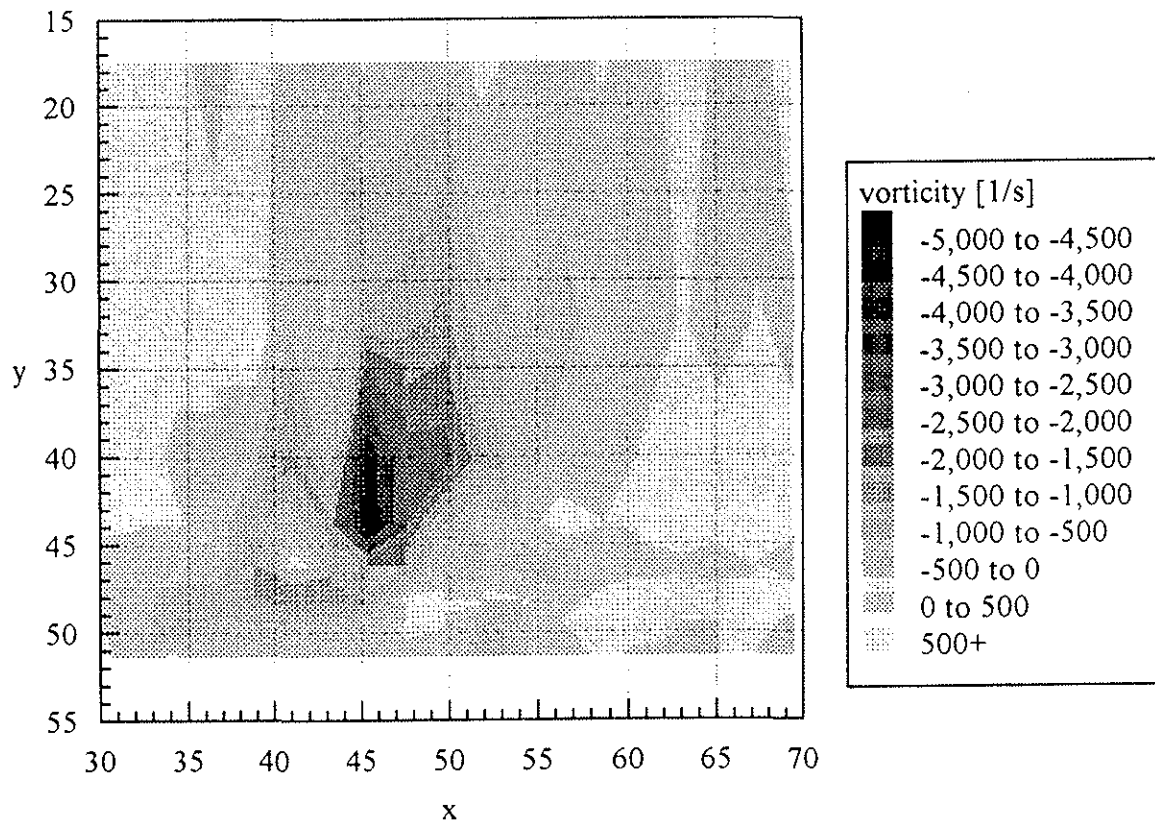


Fig. 11a Vorticity contours (reference blade)

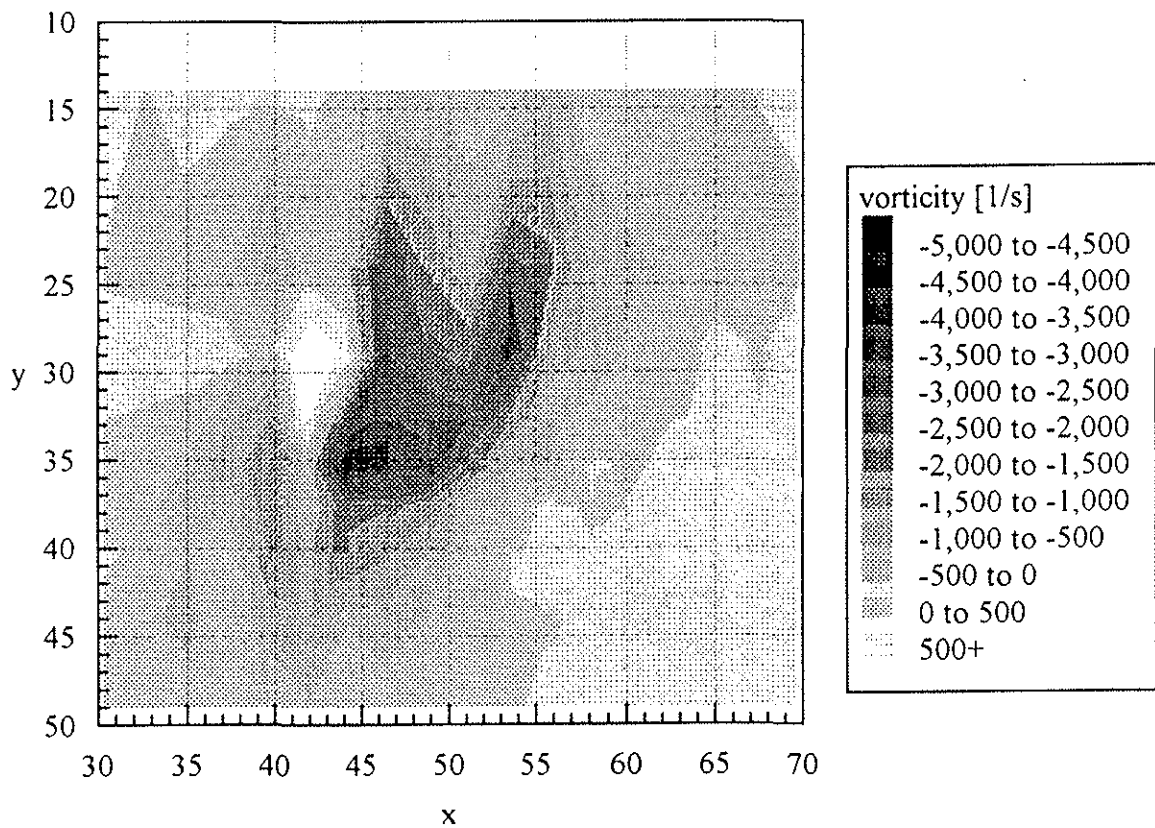


Fig. 11b Vorticity contours (winglet)

Comparing the axial velocities given in Fig. 12 it was found that the velocity deficit in the center of the vortex is much greater with the winglet. This indicates that the winglet vortex is less stable [10].

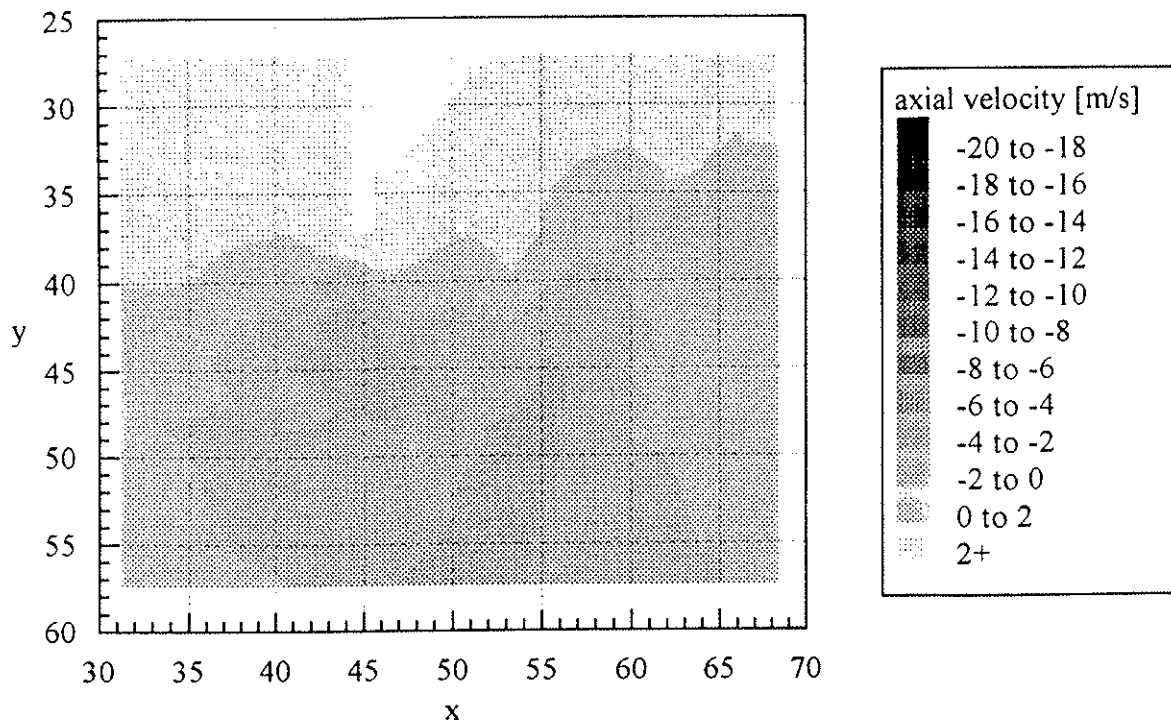


Fig. 12a Axial velocities (reference blade)

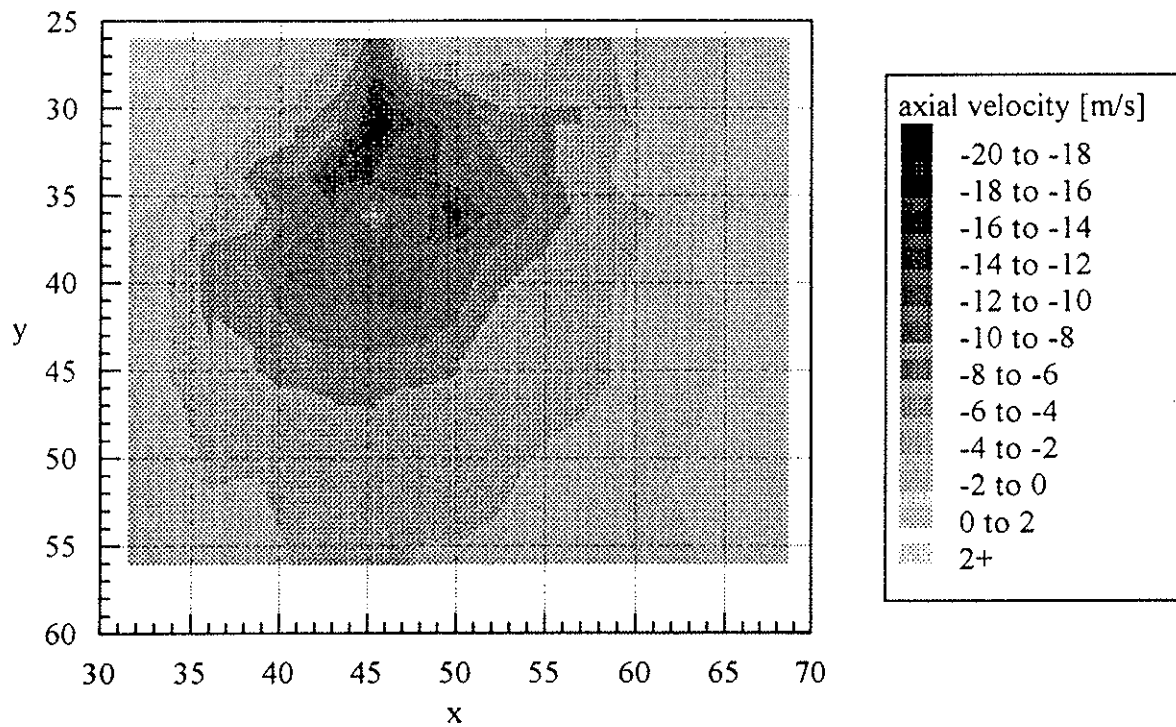


Fig. 12b Axial velocities (winglet)

4.2 blade position

At 85° azimuth position of the rotor blade the change of blade altitude relative to the rotor plane is registered by the position monitoring system. For the reference blade an average displacement of 6.8 mm in y-direction was detected at a radial position of 0.95%. The displacement of the winglet blade at the same radial location was only 0.8 mm in y-direction. These displacements are taken into account for all the calculations of vortex positions relative to the rotor plane.

4.3 vortex formation

Fig. 13 shows the measuring grid in the y-z-plane for the reference and winglet blade with the expected locations of the created blade tip vortex and the 90° old tip vortex of the preceding blade.

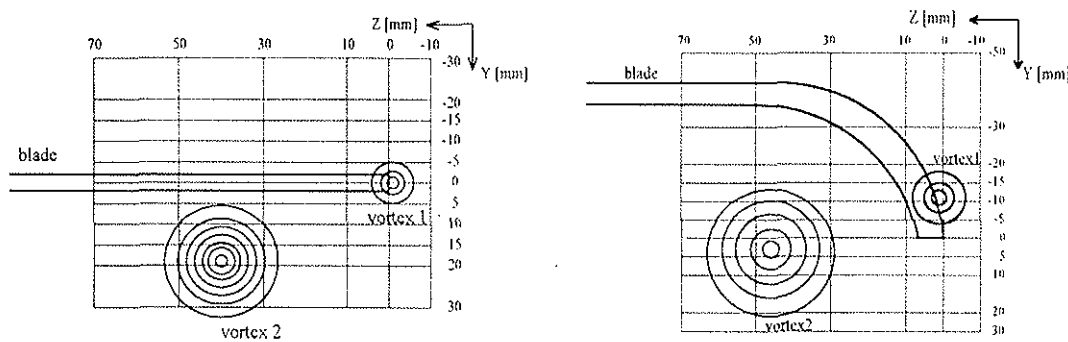


Fig. 13 Grid at 90°

Analysing the measured flow field, first of all vortex movements have been investigated. The vorticity contours at different times give a good idea of vortex roll up and vortex aging. Taking the maximum of the obtained vorticity ω_x of the new generated tip vortex in each of the y-z-planes behind the blade gives information about the temporal development ($d\omega_x/dt$) of the formation process for the different tip vortices. Fig. 14a shows the development of the maximum vorticity for the reference and winglet blade tip vortices. For the reference blade the total maximum vorticity is 20% higher than for the winglet vortex and also the maximum is reached earlier. This can clearly be seen in the gradient ($d\omega_x/dt$) of the vortex strength for the two different vortices (Fig. 14b). For the reference blade vortex $d\omega_x/dt$ reaches zero after 0.52 ms (about 5° of azimuth). Now the maximum of the vortex strength is reached and the dissipation of the vortex starts. For the winglet blade vortex $d\omega_x/dt = 0$ is reached after 0.7 ms and dissipation starts later than for the reference blade vortex. The dissipation rates for both vortices are almost equal.

In addition to the vorticity the axial velocity component in the vortex center is an indication for the stability of a vortex [10]. The temporal development of the axial velocity at the position of the maximum vorticity is depicted in Fig. 15. It is obvious, that the axial velocity of the reference blade tip vortex is higher than the axial velocity of the winglet blade tip vortex. This is in agreement with the course of the vortex strength. The reference blade seems to create a jet in the center of the tip vortex. This indicates a very stable vortex. The jet decreases in a short time and later both vortices show about convection velocity.

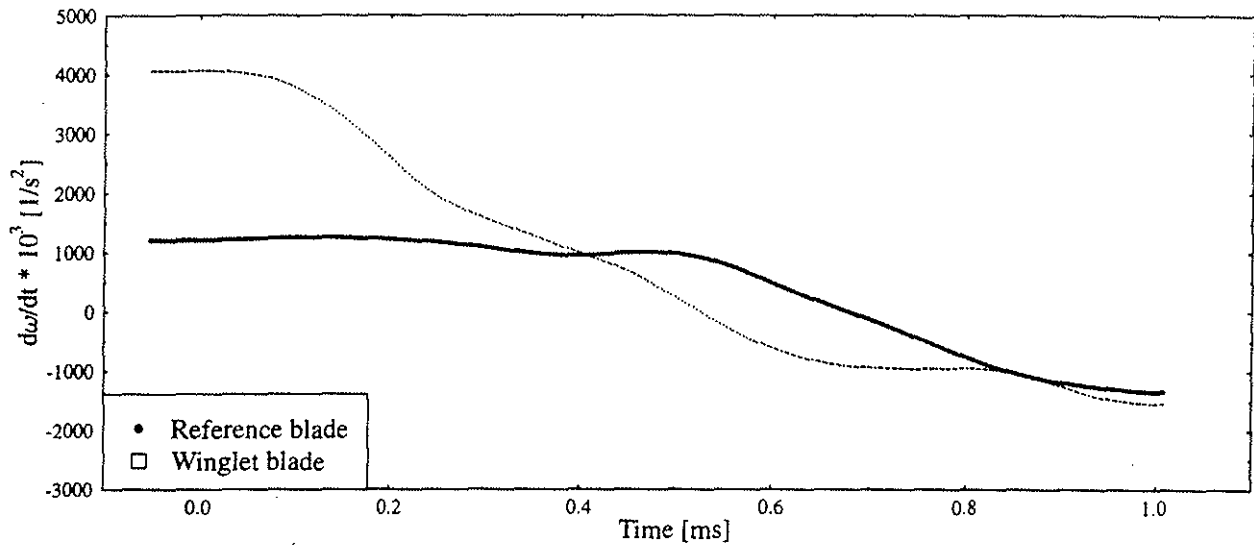
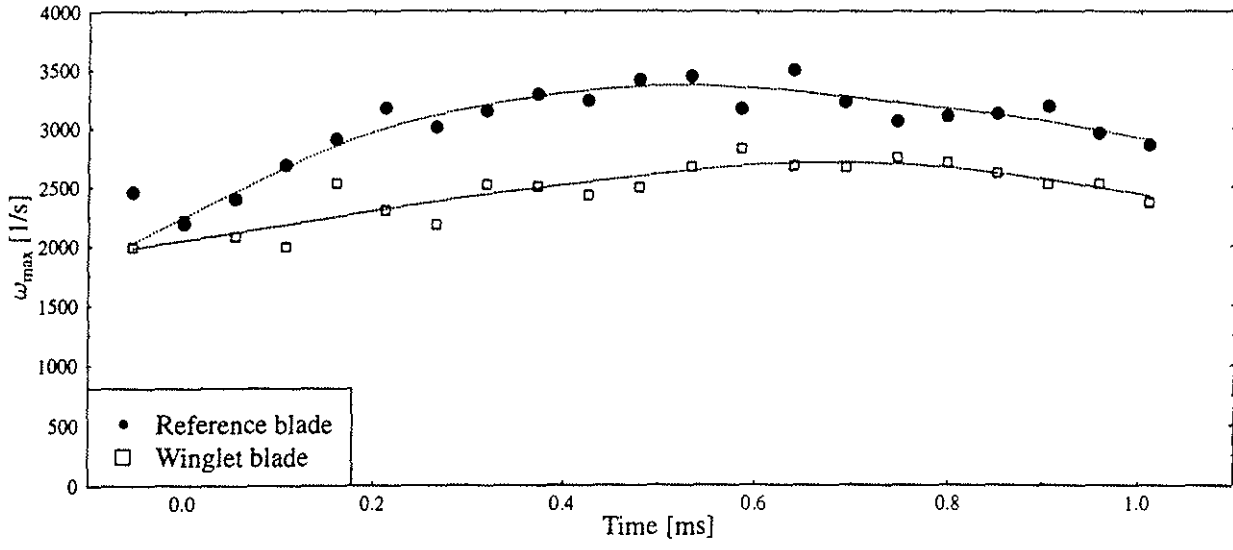


Fig. 14 Development of maximum vorticity

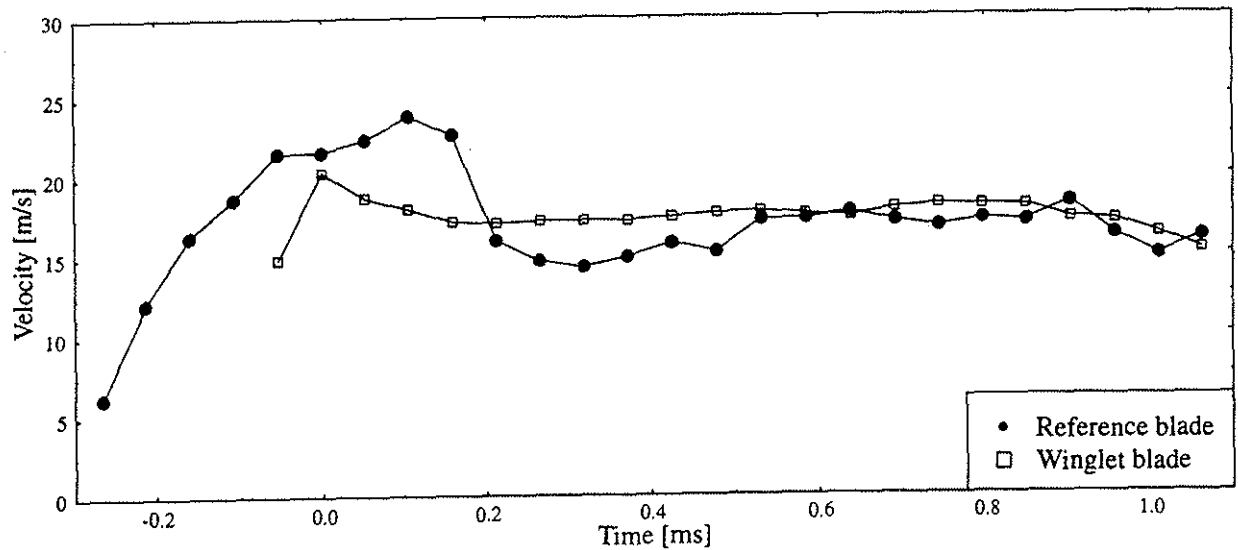


Fig. 15 Development of axial velocity

4.4 BVI parameter

Position of vortex roll up

Assuming the position of the maximum vorticity as the vortex center, this information gives access to the location of the vortex relative to the rotor plane. For the reference blade the position of vortex generation is found to be 4 mm above the rotor plane. For the winglet blade the location of vortex generation is 30 mm below the rotor plane at 70% of the winglet depth. The increase of blade-vortex miss distance by using winglets has been known from flow visualization experiments, but the LDV data give more accurate values.

Interaction geometry

To investigate the interaction geometry of the preceding blade tip vortex with the blade at 90° azimuth, the x-component of the vorticity ω_x is a good indication. First, the distance of the preceding blade vortex relative to the blade at 90° azimuth can be evaluated from the data. The vorticity contours in the y-z-plane in front of the blade show only the vorticity of the vortex from the preceding blade. For the reference blade (Fig. 16a) the location of the maximum vorticity with -2300 s^{-1} is 10 mm above the rotor blade and at a radial position of 0.95%. In the y-z-plane directly after the blade passage (Fig. 16d), the vorticity maximum has decreased to -1510 s^{-1} and is located 3 mm above the blade and at the radial position of 0.91% rotor radius. In addition, some positive vorticity appears at a radial position of 0.95% and 7mm below the blade.

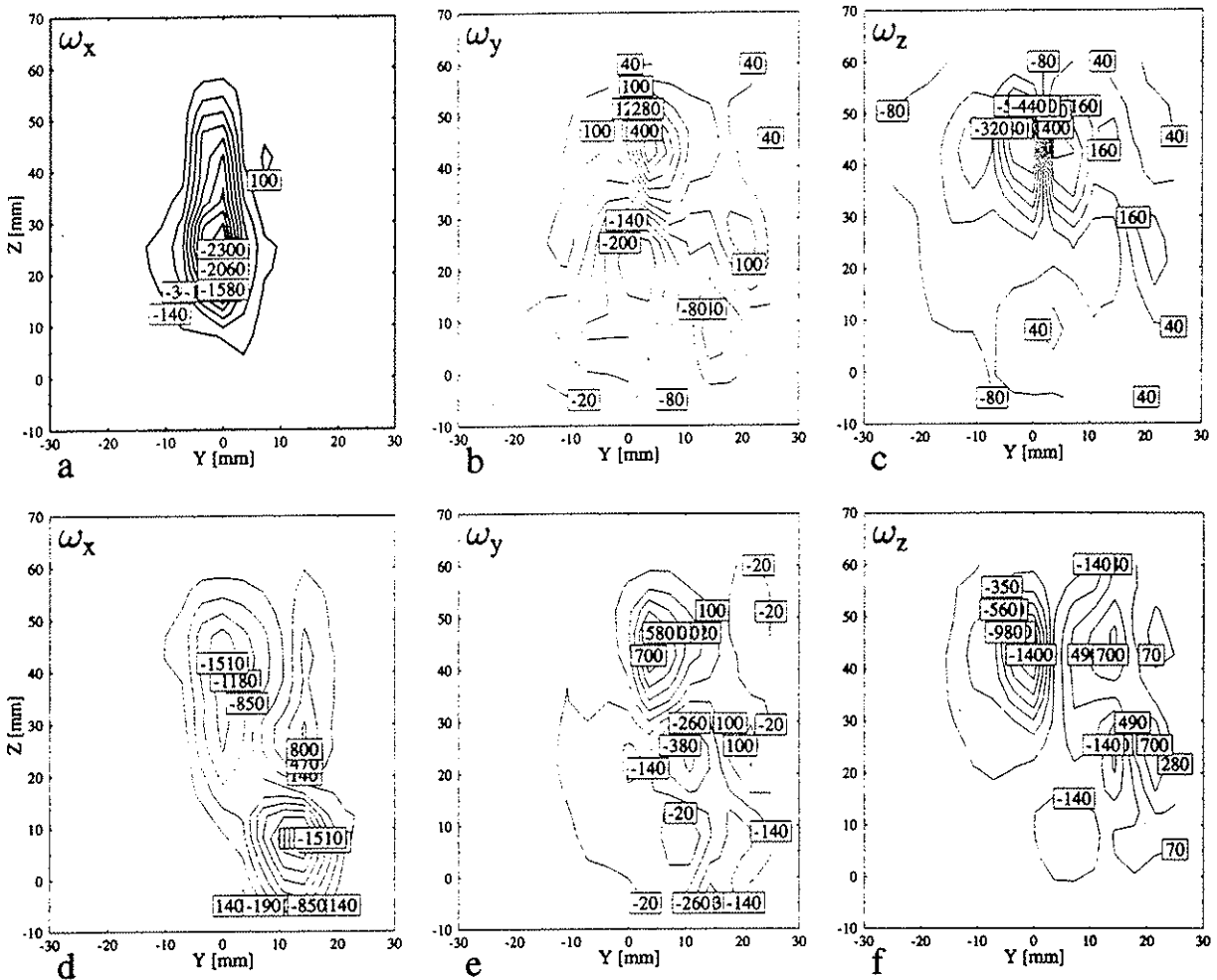


Fig. 16 Vorticity contours (reference vortex)

The vorticity contours of the preceding winglet blade tip vortex in front of the blade show a weak maximum of -700 s^{-1} at 0.91% radial position (Fig. 17a). The position is 10 mm below the rotor plane. After interaction with the rotor blade no significant vorticity can be detected (Fig. 17d).

Looking to the three dimensional vorticity distribution gives explanations for the lost of the vorticity ω_x for the reference blade. Vorticity components ω_y and ω_z in the y-z-plane in front of the blade have no significant amount (Fig. 16b,c). In addition to the decrease of ω_x from -2300 s^{-1} to -1500 s^{-1} in the y-z-plane behind the blade there is an increase in the y and z component of the vorticity to $\omega_y = 750 \text{ s}^{-1}$ and $\omega_z = -1450 \text{ s}^{-1}$ (Fig. 16e,f). The total vector of the vorticity has still a strength of -2200 s^{-1} . The orientation of the vortex axis after the interaction with the blade has changed to nearly 45° in the x-z-plane. A vortex deformation by BVI has been found by flow visualization earlier [11]. Due to the weak vortex of the 90° old winglet tip vortex and the larger distance to the blade, there are no significant vorticity components left after the interaction with the blade (Fig. 17b,c,e,f).

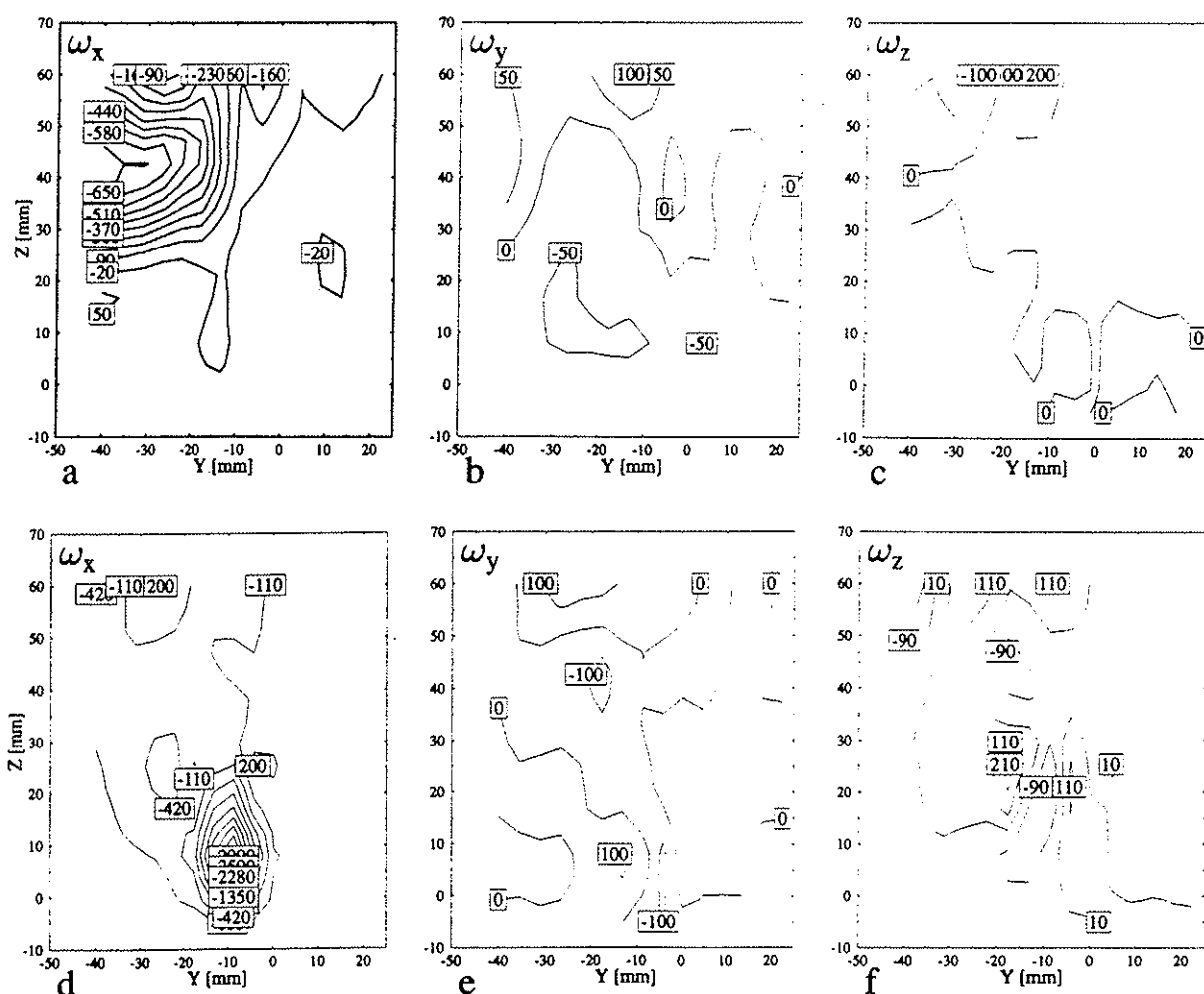


Fig. 17 Vorticity contours (winglet vortex)

Bound circulation

In addition to the vorticity the bound circulation can be calculated from the data set. Therefore the time information is converted into spatial co-ordinate by equation (2). For the six different radial positions the circulation is calculated around the wing on a rectangular box in x- and z-

direction. The results are shown in Fig. 18. The circulation profile of the reference blade (Fig. 18a) shows a local minimum at $r/C = 0.7$. This local minimum is created by the perpendicular blade vortex interaction at this location. The occurrence of a strong gradient with different sign in the circulation profile leads to the appearance of vorticity with different sign in the vorticity distribution, shown in Fig. 16d. This vortex has also been detected in stationary measurements [9] on the same profile. For the circulation profile of the winglet blade (fig 18b) only a weak gradient in the circulation profile at $r/C=0.7$ can be seen. Due to this weak gradient, no vorticity with opposite sign can be detected in the vorticity distribution (fig 17d).

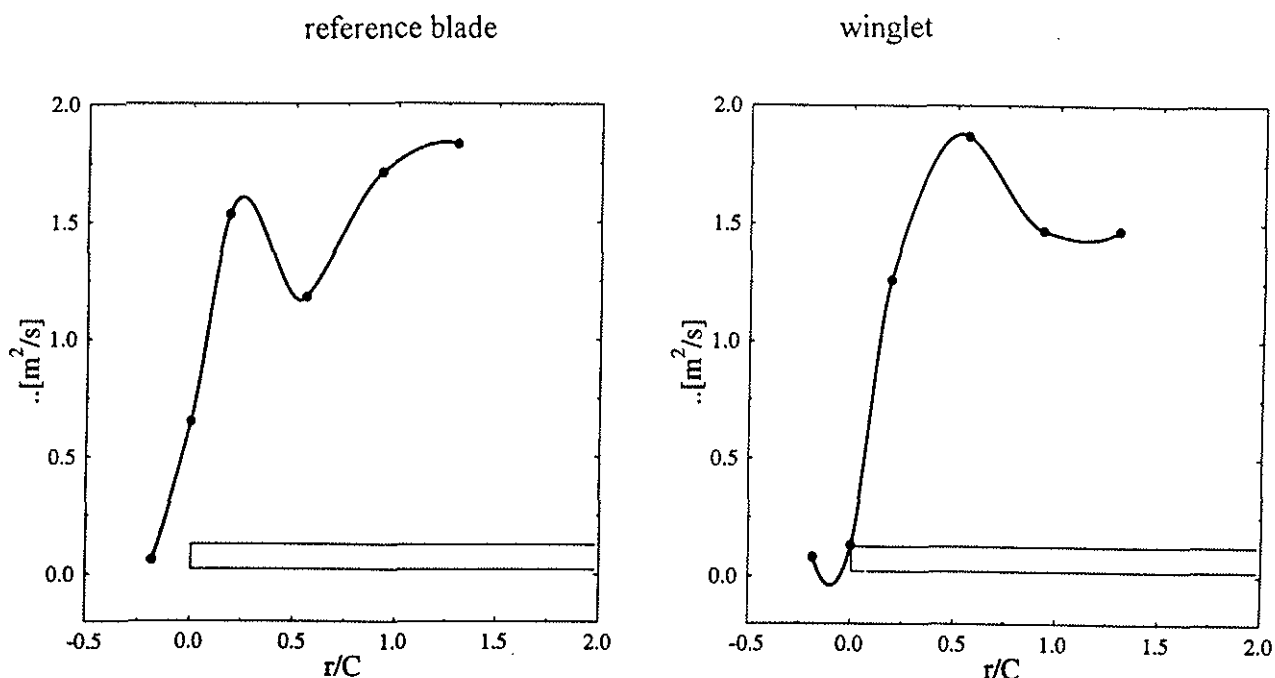


Fig. 18 Bound circulation distribution

5. Conclusions

Wind tunnel tests have been performed to measure the vortex structure of a rotor in forward flight. The measurement of the local flow vector at positions within the plane of rotation of a helicopter rotor can only be performed with a nonintrusive measuring technique. A large three component Laser-Doppler-Velocimeter was used for this purpose. The totally new conception of the LDV brings a lot of progress concerning sensitivity, data rate and third component resolution. A 'position monitoring system' gives access to blade motion parameter (lead-lag motion, pitching and angle of incidence) at any chosen radial position of the blade, where LDV measurements are performed. This is necessary to determine the distance of the probe volume in relation to the blade surface for average displacement as well as for the unsteady motion of the blade during the passage of the measurement station. The tests were run with a 1.02 m rotor having NACA 0015 airfoils with square tips or so called winglets (non-planar blade tips designed in Aachen).

Measurements were performed in two planes perpendicular to the rotor plane, one at 0° of azimuth the other at 90° . Vectot plots gave first information about position and extent of the vortices. Velocity distributions were used to obtain vortex data like core radius or maximum tangential velocities. The vortex core radius of the square tip was examined to 8.9% of blade chord or 0.94% of rotor radius, which is larger than often expected. All data are compared for

both blades to determine the influence of winglets on vortex structure and vortex roll up. Analysing the measured flow field vortex movements have been investigated. The increase of blade-vortex miss distance by using winglets has been determined exacter than from flow visualisation experiments. The vorticity contours at different times gave a good idea of vortex roll up and vortex aging. Many results indicated a surprisingly high amount of 'out of plane' vorticity in ω_y and ω_z . These were created by vortex deformation during BVI. The square tip showed a very fast roll up of the vortex and the maximum vorticity was reached about 5° of rotation after blade passage. The following decrease of max. vorticity due to aging was moderate. The winglet vortex rolled up much slower, its maximum vorticity was found 20% less and the vortex aging seemed to be the same compared to the reference blade.

References

1. M.V. Lawson, Progress towards quieter civil helicopters, Forum Proceedings of the 17th European Rotorcraft Forum, Paper No. 91-59, Berlin, Germany, Sept. 1991
2. J.M. Gallman, A parametric computational study of isolated blade vortex interaction noise, Conference Proceedings of the 14th Aeroacoustics Conference, Paper No. 119, Aachen, Germany, May 1992
3. A. Desopper, P. Lafon, J.J. Philippe and J.Prieur, Effect of an anhedral sweptback tip on the performance of a helicopter rotor, Vertica, Vol 12, No.4, pp. 345-355, 1988
4. R.H.G. Müller, Winglets on rotor blades in forward flight - a theoretical and experimental investigation, Vertica, Vol.14, No.1, 1990
5. U. Seelhorst, K.A. Bütefisch, K.H. Sauerland, Three component Laser-Doppler-Velocimeter development for large wind tunnel, ICIASF '93 Record, pp. 33.1-33.7, 1993
6. P. Thomas, On the influence of Basset history force on the motion of a particle through a fluid, Phys. Fluid A4 (9), September 1992, pp. 2090-2093
7. H. Grauer-Carstensen, A Versatile Model Position Monitoring System, DLR IB 222 - 91 A 32
8. B.M.J. Beesten, Influence of non-planar blade tips on rotor performance, Forum Proceedings of the 18th European Rotorcraft Forum, Paper No. 73, Avignon, France, Sept. 1992
9. R.H.G. Müller, Special vortices at a helicopter rotor blade, Journal of the American Helicopter Society, Vol.35, No.4, Oct. 1990
10. S. Leibovich, Vortex stability and breakdown: Survey and extension, AIAA 1983, Vol. 22, No. 9, pp 1192-1206
11. B.M.J. Beesten, On the Influence of Blade-Vortex-Interactions on Vortex Structure, Forum Proceedings of the 16th European Rotorcraft Forum, Paper No. II.10.3, Glasgow, Scotland, Sept. 1990